The Astrophysical Journal, 720:1569–1576, 2010 September 10 doi:10.1088/0004-637X/720/2/1569

A CORRELATION BETWEEN STELLAR ACTIVITY AND HOT JUPITER EMISSION SPECTRA*

Heather A. Knutson[1,3], Andrew W. Howard[1,2,4], and Howard Isaacson[1]
[1] Department of Astronomy, University of California, Berkeley, CA 94720-3411, USA; hknutson@berkeley.edu
[2] Space Sciences Laboratory, University of California, Berkeley, CA 94720-7450, USA
Received 2010 April 14; accepted 2010 July 21; published 2010 August 23

ABSTRACT

We present evidence for a correlation between the observed properties of hot Jupiter emission spectra and the activity levels of the host stars measured using Ca II H & K emission lines. We find that planets with dayside emission spectra that are well-described by standard one-dimensional atmosphere models with water in absorption (HD 189733, TrES-1, TrES-3, WASP-4) orbit chromospherically active stars, while planets with emission spectra that are consistent with the presence of a strong high-altitude temperature inversion and water in emission orbit quieter stars. We estimate that active G and K stars have Lyman α fluxes that are typically a factor of 4–7 times higher than quiet stars with analogous spectral types and propose that the increased UV flux received by planets orbiting active stars destroys the compounds responsible for the formation of the observed temperature inversions. In this paper, we also derive a model-independent method for differentiating between these two atmosphere types using the secondary eclipse depths measured in the 3.6 and 4.5 μm bands on the *Spitzer Space Telescope* and argue that the observed correlation is independent of the inverted/non-inverted paradigm for classifying hot Jupiter atmospheres.

Key words: binaries: eclipsing – planetary systems – stars: activity – techniques: spectroscopic

1. INTRODUCTION

The close-in, gas giant planets known as "hot Jupiters" occupy a unique regime of parameter space, with temperatures between 1000 and 2500 K and atmospheric compositions that are likely to be quite different than those of the cooler solar system gas giants. Because the time scale for tidal synchronization is short compared to the ages of these systems, hot Jupiters in circular orbits are expected to be tidally locked, leaving one side of the planet in permanent darkness while the other is constantly illuminated by intense radiation from the star. This further complicates the atmospheric chemistry, as the cooler night side may act as either a source or a sink for different materials, while vigorous day-night circulation may produce increased vertical mixing on the dayside. These planets also experience much higher UV fluxes than the solar system gas giants, and it is likely that photochemistry alters the atmospheric chemistry down to pressures of 10 mbar or more (Liang et al. 2003, 2004; Zahnle et al. 2009, 2010; Line et al. 2010). Infrared light from these planets emerges from pressures of 10–100 mbar (e.g., Burrows et al. 2008; Showman et al. 2009), and as a result their dayside emission spectra could exhibit strong features from photochemically produced molecules. Indeed, the detection of an excess of CO_2 in the atmosphere of the hot Jupiter HD 189733b (Swain et al. 2009a) indicates that non-equilibrium chemistry may play an important role in these atmospheres.

We can characterize the dayside emission spectra of these planets by measuring the wavelength-dependent decrease in light, as the planet passes behind the star in an event known as a secondary eclipse. Secondary eclipse observations have now been carried out for more than sixteen extrasolar planets, and there is currently a growing body of evidence for the existence of two distinct classes of hot Jupiter atmospheres (see Deming 2008, and references therein). According to the current classification scheme, one class of planets (e.g., HD 189733; Charbonneau et al. 2008) have dayside emission spectra that are well-described by atmosphere models with water and CO in absorption. A second class of planets (e.g., HD 209458; Knutson et al. 2008) are better described by models with a strong temperature inversion between 0.1 and 0.01 bars and these same features in emission.

We do not know the nature of the absorber required to create these inversions; it was initially suggested that gas-phase TiO might provide the necessary opacity (Hubeny et al. 2003; Burrows et al. 2007, 2008; Fortney et al. 2006, 2008), but this theory cannot explain the full range of current observations. TrES-3 is hot enough for gas-phase TiO but does not appear to have an inversion (Fressin et al. 2010), whereas XO-1 receives a much lower incident flux comparable to that of HD 189733b and yet has an inversion (Machalek et al. 2008). It is also unclear whether or not TiO can be reliably maintained in the upper atmosphere at all, given its high molecular weight and the likely presence of dayside and night side cold traps. Overcoming these effects would require vigorous mixing, but this may not be expected in a stably stratified atmosphere (Spiegel et al. 2009). More recently, Zahnle et al. (2009) presented detailed non-equilibrium atmospheric chemistry models suggesting that heating from sulfur compounds in the upper atmospheres of hot Jupiters could explain these inversions; in this model, photochemistry serves as a net sink for the sulfur compounds of interest.

In order to quantify the effects of photochemistry in these atmospheres more precisely, we must first obtain an estimate of the incident UV flux. Direct measurements of the stellar UV fluxes are only available for a handful of systems, including HD 189733b (Lecavelier des Etangs et al. 2010) and HD 209458b (Vidal-Madjar et al. 2003, 2004; Ehrenreich et al. 2008; France et al. 2010; Linsky et al. 2010), while archival searches for X-ray detections (Kashyap et al. 2008) and more recent observations of planet-hosting stars with *XMM-Newton* (Poppenhaeger et al. 2010) provide only upper limits in most cases. In this paper we present measurements of Ca II H & K line

* Based on observations obtained at the W. M. Keck Observatory, which is operated jointly by the University of California and the California Institute of Technology. Keck time has been granted by both NASA and the University of California.
[3] Miller Fellow.
[4] Townes Fellow.

strengths (Noyes et al. 1984), which act as an indicator of stellar activity levels, based on Keck HIRES spectra for 50 transiting planet host stars. These observations allow us to identify the most active planet-hosting stars, which should have correspondingly enhanced UV and X-ray fluxes (e.g., Schrijver et al. 1992; Livingston et al. 2007), and to search for evidence that increased activity in the host star can explain the observed dichotomy in hot Jupiter emission spectra. We describe our observations in Section 2, and survey the available literature on classifications of hot Jupiter emission spectra in Section 3. In Section 4, we develop a model-independent metric for distinguishing between the two observed types of planetary atmospheres and argue that planets without inversions are consistently found around the most active stars, while planets with strong inversions orbit quiet stars. We then estimate the effect that increased activity has on the measured Lyman α fluxes from the stars in our sample in Section 5, and discuss the consequences this has for our understanding of hot Jupiter atmospheres in Section 6.

2. KECK/HIRES Ca II OBSERVATIONS

We observed the transiting planet host stars listed in Table 1 with the HIRES echelle spectrometer (Vogt et al. 1994) on the 10 m Keck I telescope (see Figures 1 and 2). We used the standard HIRES setup employed by the California Planet Search (CPS) group (Wright et al. 2004; Howard et al. 2009). Most observations were made with a slit of width 0.″86 for 500 s yielding a signal to noise of 75–200 per pixel (depending on the host star brightness). Many of the observations were initially made for radial velocity monitoring, and additional single-exposure observations were obtained wherever possible to expand this coverage to a larger sample of transiting planet host stars. For the radial velocity observations, an iodine cell was mounted directly in front of the spectrometer entrance slit to provide a wavelength scale and calibration of the instrumental profile (Marcy & Butler 1992; Valenti et al. 1995). The iodine absorption lines (5000–6200 Å) do not affect the measurement of Ca II H & K indices (3968 Å and 3933 Å). Stellar parameters were determined using an LTE spectral synthesis routine (SME or Spectroscopy Made Easy; Fischer & Valenti 2005) on observations taken without the iodine cell wherever available. Systems with only a single spectrum were observed in this mode.

We calibrate the stellar activity indices to the Mt. Wilson S-value scale, defined as the ratio of the sum of the flux in the cores of the Ca II H & K lines to the sum of two continuum bands, one redward and one blueward of the H and K lines (Wilson 1968). The calibration from flux to $S_{\rm HK}$ was accomplished using stars that were observed in both the Mt. Wilson H-K project (Duncan et al. 1991) and the California Planet Search. $S_{\rm HK}$ values for a particular star on the CPS scale are typically within 10% of the Mt. Wilson scale (Isaacson et al. 2010). Before extracting the H line at 3968.5 Å, the K line at 3933.7 Å and continuum flux levels, the spectra are shifted to rest wavelengths through a cross correlation of the National Solar Observatory (NSO) solar atlas. The flux in the H and K line cores is measured in two 1 Å FWHM weighted triangles centered on the H and K lines. The continuum sections are each 20 Å wide and reside sufficiently far away from the H and K line centers so as to avoid the broad wings of either line. After calculating the S-value for each star, we convert to $\log(R'_{\rm HK})$ using the $B-V$ color of the star (Noyes et al. 1984); this effectively removes any dependencies on the bolometric flux of the star and allows us to accurately compare the chromospheric emission from different spectral types. In cases where we have

Table 1
Ca II H & K Line Strengths

Star	$T_{\rm eff}$[b] (K)	$v \sin i$[b]	$B-V$	$S_{\rm HK}$[f]	$\log(R'_{\rm HK})$[f]
HD 17156	5980	4.3	0.64	0.155	−5.022
HD 147506	6260	20.7	0.41	0.191[e]	−4.780
HD 149026	6150[c]	6.2	0.61	0.152	−5.030
HD 179949	6170	7.0	0.50	0.232	−4.622
HD 189733	5090	2.7	0.93	0.508	−4.501
HD 209458	6070	4.0	0.59	0.160	−4.970
HD 80606	5510	2.4	0.77	0.154	−5.061
GJ 436	3590[c]	<3	1.52	0.620	−5.298
υ And	6160[c]	9.7	0.54	0.156	−4.982
TrES-1	5300	0.5	0.78	0.244	−4.738
TrES-2	5840	1.6	0.62	0.165	−4.949
TrES-3	5530	3.1	0.71	0.305	−4.549
TrES-4	6200[c]	8.5	0.52	0.141	−5.104
XO-1	5750[c]	1.1	0.69	0.168	−4.958
XO-2	5340[c]	1.4	0.82	0.173	−4.988
XO-3	6430[c]	18.5	0.46[d]	0.239[e]	−4.595
XO-4	6400[c]	8.8	0.47[d]	0.124	−5.292
HAT-P-1	5980	2.2	0.58[d]	0.158	−4.984
HAT-P-3	5170	0.5	0.87[d]	0.206	−4.904
HAT-P-4	5990	5.1	0.58[d]	0.145	−5.082
HAT-P-5	5960[c]	2.6	0.59[d]	0.148	−5.061
HAT-P-6	6410	8.5	0.41	0.187	−4.799
HAT-P-7	6350	3.8	0.44	0.150	−5.018
HAT-P-8	6130	11.5	0.54[d]	0.156	−4.985
HAT-P-9	6350[c]	11.9	0.48[d]	0.141	−5.092
HAT-P-10[a]	4990	0.5	1.01	0.322	−4.823
HAT-P-11	4820	0.5	1.02	0.580	−4.567
HAT-P-12	4650	0.5	1.13[d]	0.253	−5.104
HAT-P-13	5710	2.7	0.73	0.141	−5.138
HAT-P-14	6530	8.5	0.42	0.175	−4.855
HAT-P-15	5570[c]	2.0	0.71[d]	0.166	−4.977
HAT-P-16	6160[c]	3.5	0.53[d]	0.175	−4.863
WASP-1	6170	0.2	0.53[d]	0.140	−5.114
WASP-2	5230	1.3	0.84[d]	0.159	−5.054
WASP-3	6170	14.2	0.52	0.173	−4.872
WASP-4	5500[c]	2.0	0.74[d]	0.194	−4.865
WASP-12	6300	3.0	0.50[d]	0.113	−5.500
WASP-13	5910	5.0	0.60[d]	0.127	−5.263
WASP-14	6270	3.9	0.45	0.163	−4.923
WASP-17	6380	10.7	0.48[d]	0.121	−5.331
WASP-18	6250	11.7	0.49	0.116	−5.430
WASP-19	5590	5.3	0.70[d]	0.252	−4.660
CoRoT-1	5950[c]	5.2	0.59[d]	0.124	−5.312
CoRoT-2	5630[c]	11.5	0.69[d]	0.435	−4.331
CoRoT-7	5330	2.5	0.80[d]	0.225	−4.802
Kepler-4	5860[c]	2.2	0.62[d]	0.168	−4.936
Kepler-5	6300[c]	4.0	0.50[d]	0.148	−5.037
Kepler-6	5650[c]	3.0	0.68[d]	0.160	−5.005
Kepler-7	5930[c]	4.2	0.59[d]	0.155	−5.099
Kepler-8	6210[c]	10.5	0.52[d]	0.153	−5.050

Notes.

[a] Also known as WASP-11.

[b] Values for $T_{\rm eff}$ (K) and $v \sin i$ (km s^{-1}) were determined from a SME analysis of the Keck/HIRES spectra as described in Fischer & Valenti (2005) when available, otherwise values from the literature were used instead.

[c] We revert to the published values for stellar effective temperature and $v \sin i$ in these cases.

[d] In some cases, measured $B-V$ values were unavailable or were inconsistent with the star's spectral type. In these cases, we opted to set the $B-V$ color for each star equal to the value given in Table B.1 in Gray (2005) for a given effective temperature. We do not account for variations in $B-V$ due to metallicity or age, as these quantities have a negligible effect on our final $\log(R'_{\rm HK})$ values for the range of stellar spectral types present in our sample.

[e] These hot, rapidly rotating F stars have $S_{\rm HK}$ and $\log(R'_{\rm HK})$ values that are suggestive of activity but they are near the edge of the range in $B-V$ for which these indices are calibrated, and their spectra show no detectible emission in the Ca II H & K line cores. We argue in Section 2.1 that these stars are most likely chromospherically quiet.

[f] $S_{\rm HK}$ and $\log(R'_{\rm HK})$ values are only calibrated for stars with $B-V$ between 0.5 and 1.4 (4200 and 6200 K). We give values for all of the stars in our sample, but values for spectral types outside this range should be treated with some skepticism.

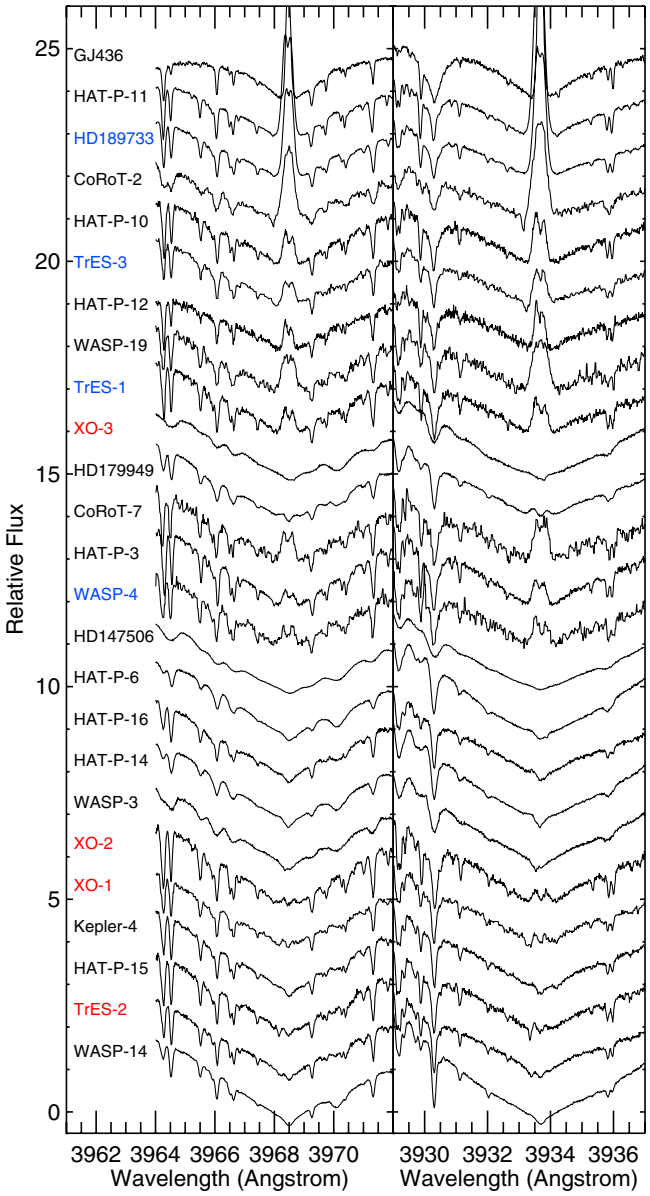

Figure 1. Ca II H & K lines for transiting planet host stars observed with Keck/HIRES, plotted in order of increasing $S_{\rm HK}$. This plot shows half of our sample, with the second half plotted in Figure 2. Active stars have significant emission in the line cores (high values of $S_{\rm HK}$) and lie at the top of the plot; a majority of the stars in our sample appear to have no detectible emission. Star names are given on the left, with systems hosting planets with temperature inversions shown in red and those without temperature inversions shown in blue, while names in black denote systems with insufficient data. It is possible that cooler (<1000 K) and/or higher density planets, such as the Neptune-mass planets GJ 436 and HAT-P-11, may not fit into the simple classification scheme used to describe hot Jupiter atmospheres (indeed this appears to be the case for GJ 436; Stevenson et al. 2010), but we include HIRES observations in this plot wherever available for completeness.

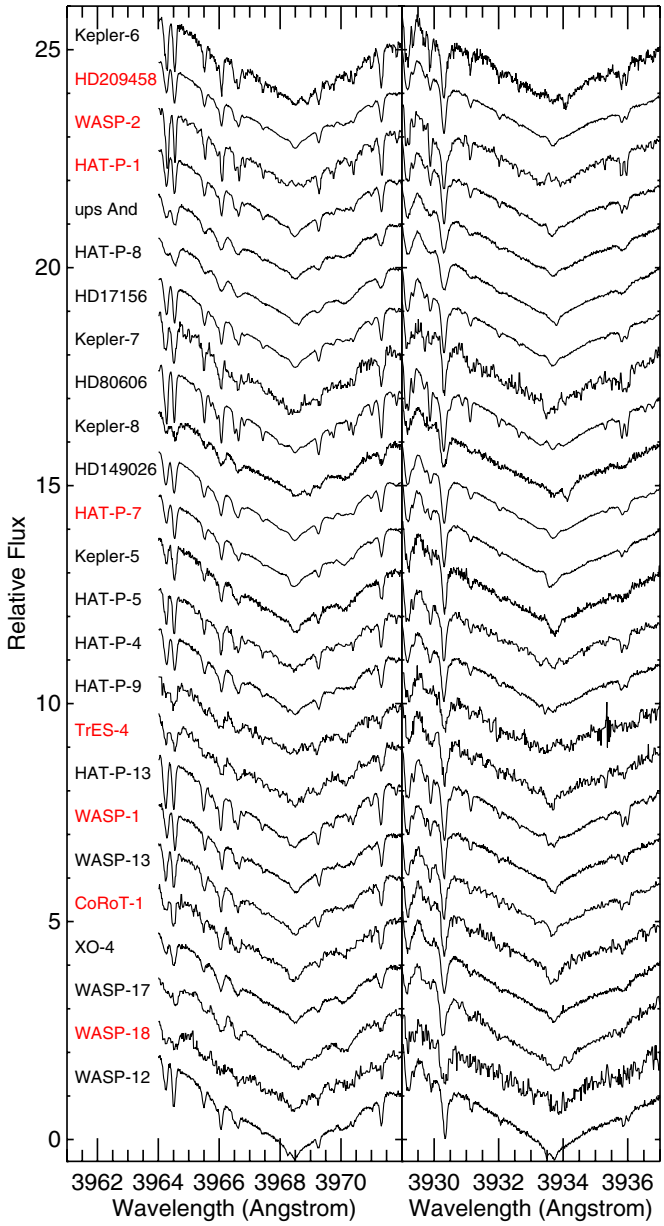

Figure 2. Ca II H & K lines for transiting planet host stars observed with Keck/HIRES, plotted in order of increasing $S_{\rm HK}$. This plot is a continuation of Figure 1 and includes stars with lower values of $S_{\rm HK}$.

multiple spectra available spanning several epochs, we take the median value of $\log(R'_{\rm HK})$ over all of the available observations. We list the resulting $S_{\rm HK}$ and $\log(R'_{\rm HK})$ values in Table 1; for a more detailed description of our observations and methodology see Isaacson et al. (2010).

2.1. $S_{\rm HK}$ and $\log(R'_{\rm HK})$ for F Stars

Although we calculate $S_{\rm HK}$ and $\log(R'_{\rm HK})$ values for the F stars ($T_{\rm eff}$ = 6000–6500 K) in our sample, we note that the $\log(R'_{\rm HK})$ scaling relations described in Noyes et al. (1984) are not well calibrated for $B-V < 0.5$. Because F stars have higher continuum fluxes in the region of the Ca II H & K lines, it can be difficult to detect small amounts of emission in the line cores even when it is present. Our values for $S_{\rm HK}$ and $\log(R'_{\rm HK})$ for XO-3 ($T_{\rm eff}$ = 6430 K, $v \sin i$ = 18.5 km s^{-1}) and HD 147506 ($T_{\rm eff}$ = 6260 K, $v \sin i$ = 20.7 km s^{-1}) suggest that both stars are active, but these values should be regarded with some suspicion as these stars are on the edge of the calibrated range in $B-V$.

As an additional test, we carried out a visual inspection of the spectra for XO-3 and HD 147506 and could find no evidence for emission in the Ca II H & K line cores. It is possible that the rotational broadening could be obscuring the presence of weak lines; we test this theory by searching the database of all CPS spectra and selecting a sample of F stars with effective temperatures and $S_{\rm HK}$ values similar to those of XO-3 and HD 147506 ($6000 < T_{\rm eff} < 6500$ K, $0.18 < S_{\rm HK} < 0.24$), but with significantly lower (<7 km s^{-1}) values of $v \sin i$. We

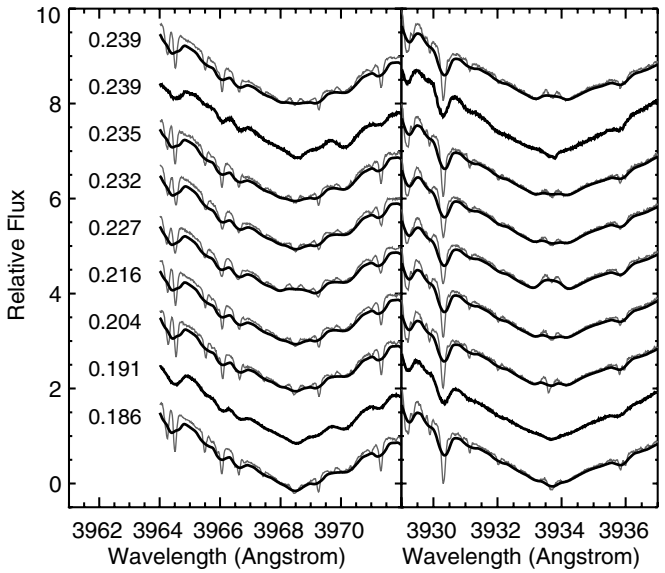

Figure 3. Ca II H & K lines for a sample of seven F stars observed with Keck/HIRES as part of ongoing CPS programs, plotted in order of increasing S_{HK} (values given on left). These stars were selected to have effective temperatures between 6000 and 6500 K, $v \sin i$ less than 10 km s^{-1}, and S_{HK} values in the range 0.18–0.24, comparable to the values measured for XO-3 ($S_{HK} = 0.239$) and HD 147506 ($S_{HK} = 0.191$). The original spectra (thin gray lines) for these stars were then artificially broadened to a $v \sin i$ of 20 km s^{-1} (thick black lines), comparable to that of XO-3 (second from top) and HD 147506 (second from bottom) which are plotted for comparison. The effective temperatures for the stars shown in this plot are, from bottom to top, 6170, 6080, 6260, 6090, 6130, 6090, 6190, 6430, and 6090 K, respectively.

then artificially broaden these spectra to a $v \sin i$ of 20 km s^{-1}, comparable to that of XO-3 and HD 147506, using the standard IDL routine lsf_rotate.pro, available as part of the astrolib distribution and described in Gray (2005). A characteristic double-peaked emission feature is clearly detectible in the line cores of the unbroadened spectra (see Figure 3), and although this signal is obscured somewhat by the broadening, there is still a noticeable flattening or even an increase in flux near the centers of the line cores in the high $v \sin i$ versions of the spectra. In contrast to these systems, XO-3 and HD 147506 (also plotted in Figure 3 for comparison) both have v-shaped spectra more characteristic of quiet stars. We conclude that both stars are likely to be chromospherically quiet, with the additional caveat that the standard S_{HK} and $\log(R'_{HK})$ indices used to measure this emission are not well-calibrated and are probably not appropriate to use for stars of this spectral type.

3. OBSERVATIONS OF HOT JUPITER EMISSION SPECTRA

There are currently four planets classified in the literature as having "non-inverted" atmospheres: HD 189733b (Deming et al. 2006; Grillmair et al. 2007, 2008; Charbonneau et al. 2008; Swain et al. 2009a), TrES-1 (Charbonneau et al. 2005), TrES-3 (Fressin et al. 2010), and WASP-4 (Beerer et al. 2010). These planets have emission spectra that are consistent with standard one-dimensional cloud-free atmosphere models where temperature decreases with increasing height in the atmosphere (e.g., Barman 2008; Burrows et al. 2008; Fortney et al. 2008; Madhusudhan & Seager 2009) or display at most a weak inversion (e.g., WASP-4; Beerer et al. 2010). Models used to describe these planets exhibit CO and H_2O features in absorption, which provides a good match to the shape of their observed emission spectra in the mid-IR (3.6–24 μm). Observations of TrES-1, TrES-3, and WASP-4 are limited to a subset of the *Spitzer* IRAC bandpasses (3.6, 4.5, 5.8, 8.0 μm), which have relatively wide (0.75–2.9 μm FWHM) transmission functions and are therefore somewhat ambiguous in their interpretation, but HD 189733b has been observed at higher wavelength resolutions with both IRS on *Spitzer* (5–14 μm; Grillmair et al. 2007, 2008) and NICMOS on the *Hubble Space Telescope* (*HST*; 1.5–2.5 μm; Swain et al. 2009a). Published models for HD 189733b in which the atmospheric chemistry and pressure-temperature profiles are allowed to vary in the fit consistently find that this planet is best-described by a pressure-temperature profile that decreases with height in the atmosphere (Madhusudhan & Seager 2009; Swain et al. 2009a).

In contrast, the emission spectra of planets such as HD 209458b (Deming et al. 2005; Richardson et al. 2007; Knutson et al. 2008; Swain et al. 2009b), TrES-2 (O'Donovan et al. 2010), TrES-4 (Knutson et al. 2009), HAT-P-1 (Todorov et al. 2010), HAT-P-7 (Christiansen et al. 2010), WASP-1b (Wheatley et al. 2010), WASP-18b (Nymeyer et al. 2010), XO-1b (Machalek et al. 2008), XO-2b (Machalek et al. 2009), XO-3b (Machalek et al. 2008), and CoRoT-1b (Deming et al. 2010) are best-described by models with a stronger temperature inversion between 0.1 and 0.01 bar and water and CO bands in emission (e.g., Hubeny et al. 2003; Fortney et al. 2006, 2008; Burrows et al. 2007, 2008; Madhusudhan & Seager 2009; Spiegel & Burrows 2010). As before, our information on the majority of these systems is limited to observations in the *Spitzer* IRAC bandpasses, although HD 209458b has also been observed with IRS (Richardson et al. 2007) and NICMOS (Swain et al. 2009b) and shorter-wavelength data are available for a few additional planets (Borucki et al. 2009; Alonso et al. 2009; Snellen et al. 2009; Christiansen et al. 2010; López-Morales et al. 2010). Model fits to HD 209458b's emission spectrum in which the chemistry and pressure-temperature profiles are allowed to vary find that this planet is best-described by a model with a temperature inversion at altitude (Madhusudhan & Seager 2009; Swain et al. 2009b), consistent with the conclusions of more highly constrained models (e.g., Burrows et al. 2007).

Although Wheatley et al. (2010) classify WASP-2b as a non-inverted planet, this interpretation relies on a specific model for creating the inversion (a solar metallicity atmosphere and gas-phase TiO in local thermal equilibrium) that does not always provide a good match for the observed spectra of other planets (e.g., HD 209458b; Fortney et al. 2008). We find that this planet's emission spectrum is reasonably well-described by a simple 1840 K blackbody function and further note that it deviates from a blackbody in ways that are more characteristic of an inverted atmosphere, with a flux that is lower than predicted in the 3.6 μm band and higher in the 4.5 μm band (see Section 4). For the purposes of this paper, we therefore place this planet in the inverted class and predict that more generalized models for temperature inversions (e.g., Burrows et al. 2008; Madhusudhan & Seager 2009) should provide an improved fit to the observed features, albeit with marginal statistical significance given the relatively large uncertainties in the planet's observed emission spectrum.

Unlike the ambiguous case of WASP-2b, CoRoT-2b has a well-measured emission spectrum that does not match the predictions of either class of models (Gillon et al. 2010; Deming et al. 2010). The 8.0 μm flux for this planet is anomalously low relative to its 4.5 μm flux (for a discussion of possible

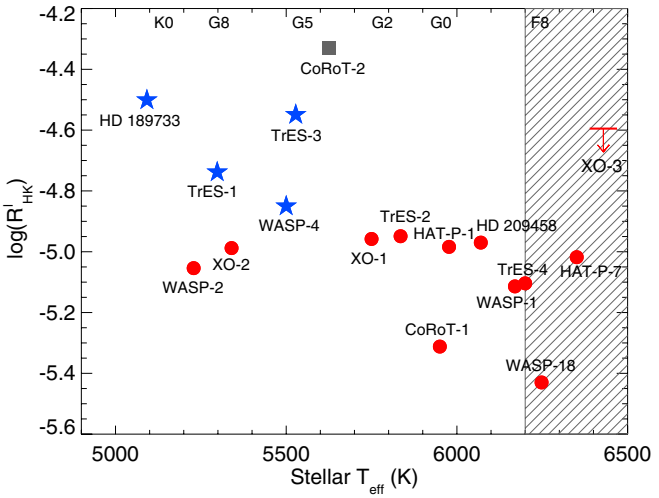

Figure 4. Stellar effective temperature vs. Ca II H & K activity index $\log(R'_{\rm HK})$, which tracks the amount of emission in the Ca II H & K line core. Active stars have stronger emission features and correspondingly large values of $\log(R'_{\rm HK})$; because the calibration for $\log(R'_{\rm HK})$ is uncertain for stars with effective temperatures higher than 6200 K (Noyes et al. 1984), we have marked this region with diagonal gray lines on this plot. Planets classified in the literature as having temperature inversions are shown as red circles, while planets in the literature that are well-described by non-inverted atmosphere models are shown as blue stars (see Section 3 for a discussion of WASP-2). CoRoT-2 (gray square) has an unusual spectrum that is not well-described by either model, and XO-3 (red downward arrow) has temperature inversion and orbits a star with a relatively high $\log(R'_{\rm HK})$ value but no visible emission in the Ca II H & K line cores by inspection (see Section 2.1). Although cooler stars tend on average to be more active, there is still a range of activity possible within a given spectral type: XO-2, WASP-2, and TrES-1 differ by less than 100 K, and yet TrES-1 is moderately active while XO-2 and WASP-2 appear to be quiet. For reference, we give the spectral types for a range of effective temperatures at the top of the plot.

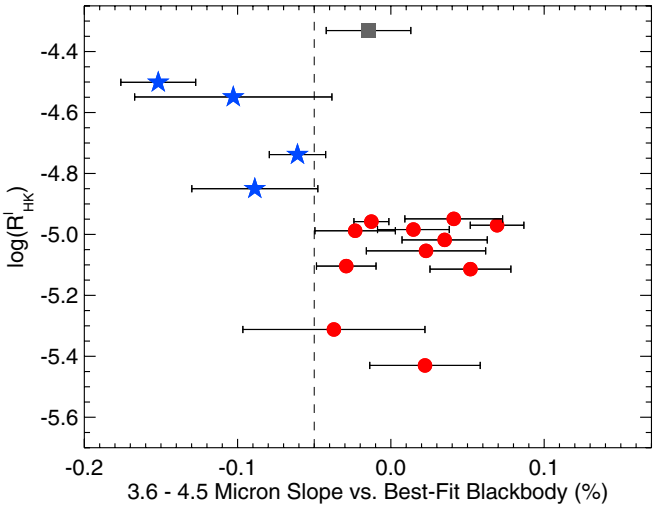

Figure 5. Empirical index for classifying hot Jupiter emission spectra vs. Ca II H & K activity index $\log(R'_{\rm HK})$. We derive our index by fitting the 3.6 and 4.5 μm secondary eclipse depths as measured in the *Spitzer* IRAC bands with a blackbody function for the planet and take the difference between the measured slope across the 3.6 and 4.5 μm bands and the value predicted by the best-fit blackbody function. Planets with blackbody emission will have an index close to zero, whereas planets with negative values are brighter than predicted at 3.6 μm and fainter at 4.5 μm, and planets with positive values have the opposite behavior. Planets classified in the literature as having atmospheric temperature inversions are shown as red circles, while planets without temperature inversions are shown as blue stars (see Section 3 for a discussion of WASP-2b). CoRoT-2b (gray square) has an unusual spectrum that is not well-described by either model, and we have excluded XO-3 from this plot as its activity level is ambiguously determined from its spectrum (see Section 2.1). The vertical dashed line at -0.05 delineates a distinction between atmosphere types; in reality there is likely a continuum of behaviors ranging from the default strong absorption (i.e., no inversion), to weak absorption (corresponding to a weak inversion), to no absorption or even emission from an increasingly strong stratosphere.

explanations, see Deming et al. 2010), and we therefore denote this planet in Figures 4 and 5 with a gray square rather than placing it in either of the two standard classes.

We exclude planets with observations in only one bandpass (e.g., HD 149026b; Harrington et al. 2007; Knutson et al. 2009), as well as systems with only ground-based observations (e.g., WASP-19b; Gibson et al. 2010; Anderson et al. 2010), as models for these planets are poorly constrained. We also exclude cooler (<1000 K), core-dominated planets such as GJ 436b and HAT-P-11b, as these planets may not fit into the simple classification scheme used to describe hot Jupiter atmospheres (indeed, this appears to be the case for GJ 436b; Stevenson et al. 2010; Beaulieu et al. 2010). We classify each of the well-characterized hot Jupiters as "inverted" or "non-inverted" according to the best-consensus interpretation available in the literature for that planet, except where otherwise noted. Figure 4 shows the stellar effective temperatures $T_{\rm eff}$ and Ca II H & K line strengths for each of these systems. We find that the "non-inverted" atmosphere types are consistently associated with the most chromospherically active stars, whereas "inverted" atmosphere types are associated with quiet stars.

4. AN EMPIRICAL METHOD FOR CLASSIFYING HOT JUPITER EMISSION SPECTRA

The classification scheme described in Section 3 relies on comparisons between the observed hot Jupiter emission spectra and one-dimensional model atmospheres for these planets. In this section, we develop a model-independent classification scheme that relies on the relative secondary eclipse depths in the 3.6 and 4.5 μm IRAC bandpasses to distinguish between atmosphere types. We select these two bands because they (1) are some of the most widely available observations for hot Jupiter atmospheres, (2) are usually the most precisely measured eclipse depths available, and (3) provide the strongest constraints on atmosphere models (e.g., Madhusudhan & Seager 2009). Because the 3.6 μm data for TrES-1 are currently unpublished, we completed a preliminary analysis of the secondary eclipse in this channel using the methods described in Knutson et al. (2009) and derive an eclipse depth of $0.085\% \pm 0.013\%$, which we use for the analysis presented here.

In order to classify each planet, we take the measured planet-star flux ratios in the 3.6 and 4.5 μm bands and fit them with a blackbody model for the planet where the temperature is allowed to vary freely. We use a PHOENIX model atmosphere (Hauschildt et al. 1999) for the star where we interpolate in $T_{\rm eff}$ and log(g) to match the star's observed properties and set the metallicity equal to zero. We calculate the predicted planet-star flux ratio in each of the *Spitzer* bands using the transmission functions provided in the Spitzer Observer's Manual and then compare the resulting predictions to the observed slope across the 3.6–4.5 μm bands. Planets with strong inversions have lower fluxes at 3.6 μm and higher fluxes at 4.5 μm compared to our best-fit blackbody function, while planets without inversions show stronger emission at 3.6 μm and weaker emission at 4.5 μm. In the models described in Section 3, this difference results from the fact that the 4.5 μm band contains both water and CO bands while the 3.6 μm band is relatively unaffected by these molecules. As these molecules switch from absorption to

emission, it alters the slope of the planet-star flux ratio across these two bands accordingly. We show the resulting difference in slopes in Figure 5, where "non-inverted" atmosphere types have negative slopes and "inverted" atmospheres have positive slopes as compared to our best-fit blackbody functions. Planets whose emission spectra are consistent with a blackbody (i.e., no significant absorption or emission) have values close to zero in this index.

This empirical classification scheme provides a good match to the "inverted/non-inverted" classifications presented in the literature, with the four planets with the most negative values in this index (HD 189733b, TrES-1, TrES-3, and WASP-4) corresponding to the "non-inverted" atmosphere types described above. Planets with significantly negative slopes across these two bands are associated with the most active stars, providing a model-independent confirmation of the proposed correlation between increased stellar activity and hot Jupiter atmosphere types. Although Wheatley et al. (2010) place WASP-2b in the non-inverted class of atmospheres, we find that our index for this planet has a value of 0.025 ± 0.039, consistent with a blackbody or slightly inverted atmosphere. As noted earlier, CoRoT-2b's anomalous emission spectrum is poorly fit by both inverted and non-inverted atmosphere models, although it is possible to fit the 3.6 and 4.5 μm eclipse depths with a 1790 K blackbody as shown in Figure 5.

5. THE CONNECTION BETWEEN CHROMOSPHERIC ACTIVITY AND UV FLUX

The observed correlation between hot Jupiter emission spectra and stellar activity levels would seem to suggest that the increased UV flux experienced by the planet destroys the high-altitude absorber responsible for the formation of temperature inversions. In order to put this correlation on a more quantitative footing, we explore the connection between Ca II H & K emission line strengths and FUV fluxes in G and K stars. We focus our study on Lyman α, as this line is generally the single strongest feature in the UV spectra of late-type stars; the sun emits as much flux in Lyman α as in all other wavelengths combined shortward of 1500 Å (Fontenla et al. 1988; Landsman & Simon 1993). In this exercise, we compare stars of similar spectral type but differing activity levels and therefore elect to work with the simpler $S_{\rm HK}$ values instead of $\log(R'_{\rm HK})$ as our activity measure. $\log(R'_{\rm HK})$ uses an empirical function of $B - V$ to remove the trend toward increasing $S_{\rm HK}$ values for later spectral types (caused by the lower continuum fluxes in the region of the Ca II H & K lines in these stars), but this correction is unnecessary when comparing stars of the same spectral type.

It is well-established that increased emission in the Ca II H & K line cores in late-type stars is an indicator of nonradiative heating processes in the chromosphere connected to the presence of enhanced magnetic fields (e.g., Leighton 1959; Noyes et al. 1984; Schrijver et al. 1989; Bailunas et al. 1985). Increased stellar activity as measured using Mg II H & K has also been observed to correlate with increased Lyman α and x-ray emission (e.g., Wood et al. 2005), but to the best of our knowledge there are no quantitative scaling laws directly relating Ca II H & K line strengths and the integrated Lyman α flux as a function of spectral type for a large sample of stars. We address this issue by selecting a sample of 26 stars with effective temperatures between 5000 and 6000 K observed in Lyman α by the *HST* STIS instrument and its precursor GHRS as described in Wood et al. (2005). For each of these stars, we obtain a measurement of the Ca II H & K emission line strengths either from Keck HIRES observations when available or from standard catalogs published in Duncan et al. (1991) and Henry et al. (1996). We also include the sun in our table, with an average Lyman α flux of 5.6×10^{-6} times its bolometric flux (Woods et al. 2000; Wood et al. 2005) and a $S_{\rm HK}$ value of 0.133 (Livingston et al. 2007). We then bin the stars into four categories according to effective temperature (5000–5500 K and 5500–6000 K bins) and activity level, where active stars are defined as those with $S_{\rm HK} > 0.3$ for the cooler temperature bin and $S_{\rm HK} > 0.2$ for the higher temperature bin. We then calculate the Lyman α fluxes corresponding to each bin using the values given in Table 3 in Wood et al. (2005), where the authors have used the Lyman α line shape information to correct for the effects of absorption from the ISM and any stellar outflows. The UV spectra used by Wood et al. are based on a collection of archival *HST* observations and tend to be biased toward more active stars; our active bins have 8 cooler stars and 11 hotter stars, while the quiet star bins each contain 4 stars.

We find that the average Lyman α flux as a fraction of the total bolometric flux is $(1.1 \pm 0.2) \times 10^{-5}$ for quiet stars between 5000–5500 K and $(4.2 \pm 0.2) \times 10^{-5}$ for active stars in that same temperature range, where the quiet stars have an average $S_{\rm HK}$ of 0.171 and the active stars have an average value of 0.545 and we set the uncertainty on the Lyman α flux estimates equal to the standard deviation of the Lyman α fluxes for the stars in that bin. This range in $S_{\rm HK}$ is comparable to the observed difference between HD 189733 (5100 K, $S_{\rm HK} = 0.508$) and its closest quiet analog WASP-2 (5230 K, $S_{\rm HK} = 0.159$). By analogy, then, we expect that HD 189733 will show an enhancement in Lyman α flux of approximately a factor of 4 relative to WASP-2. Because the two planets in these systems orbit at nearly identical distances from their host stars (0.031 AU in both cases), we expect the incident UV flux at the surface of HD 189733b to be a factor of 4 higher than at the surface of WASP-2b.

We repeat this same experiment for the 5500–6000 K temperature bins and find an average Lyman α flux of $(5.0 \pm 0.6) \times 10^{-6}$ times the bolometric flux for quiet stars and $(3.6 \pm 1.1) \times 10^{-5}$ times the bolometric flux for active stars, corresponding to a factor of 8 enhancement for an increase in average $S_{\rm HK}$ from 0.157 to 0.354. TrES-3 has an effective temperature of 5530 K and $S_{\rm HK} = 0.305$, while its closest quiet analog XO-1 has an effective temperature of 5750 K and $S_{\rm HK} = 0.168$. Taking into account the planet TrES-3b's slightly smaller orbital distance (0.023 AU vs. XO-1b's 0.049 AU), we estimate that it experiences a Lyman α flux approximately 30 times higher than that experienced by XO-1b. HD 209458 is the only planet-hosting star with a direct measurement of its Lyman α flux in Wood et al. (2005) and has a total flux of 6.9×10^{-6} times its bolometric flux, consistent with the other quiet stars in the 5500–6000 K bin.

WASP-4 (5500 K) falls on the boundary between temperature bins, but it is indistinguishable from TrES-3 (5530 K) and so we estimate its Lyman α flux using the hotter temperature bin. If we assume the Lyman α flux scales linearly with $S_{\rm HK}$, WASP-4 ($S_{\rm HK} = 0.194$) would have a Lyman α flux of 1.1×10^{-5} times its bolometric flux. Because the planet WASP-4b orbits at a comparable distance to that of TrES-3b, this means that WASP-4b would receive approximately one third the flux of this planet, ten times higher than the flux experienced by XO-1b. Comparing it to the stars in the cooler temperature bin, WASP-4b receives approximately half as much Lyman α flux as HD 189733b and twice as much as WASP-2b.

According to the empirical index plotted in Figure 5, TrES-1b lies closest to the boundary between inverted and non-inverted atmospheres, and this is reflected in its UV flux. The star TrES-1 (5300 K) has a S_{HK} of 0.244, corresponding to a Lyman α flux of 1.1×10^{-5} times its bolometric flux. This flux is comparable to that of WASP-4, but the planet TrES-1b orbits at a greater distance and as a result the incident flux at the surface of the planet is much less, only 30% greater than that received by WASP-2b.

Hot Jupiter atmospheres have a relatively high absorption cross section in Lyman α and we expect that much of this incident flux will be absorbed in the upper regions of the atmosphere, where relative abundances of molecules may differ from local thermal equilibrium by many orders of magnitude. Because photolysis cross sections and return reaction rates are species-specific and can encompass multiple pathways, it is difficult to predict a priori the effects that a significantly increased Lyman α flux would have on the relative abundance of the unknown stratospheric absorber. We suggest that this would be best addressed by comprehensive photochemistry models such as those described in Zahnle et al. (2009, 2010) and Line et al. (2010).

6. DISCUSSION & CONCLUSIONS

We measured the Ca II H & K line strengths for 50 transiting planet host stars and correlated these activity indicators with planet atmosphere type. Planets with non-inverted atmospheres are found orbiting the most chromospherically active stars, while planets with inverted atmospheres are found orbiting quiet stars. The observational correlation described above is independent of the inverted/non-inverted classification scheme for hot Jupiter atmospheres, as we find the same result for an empirical classification scheme based on 3.6 and 4.5 μm secondary eclipse depths alone. We estimate the statistical significance of our result using a rank order test in which we randomly select 4 stars out of our sample of 15 systems observed with both Keck/HIRES and *Spitzer* after excluding XO-3 and CoRoT-2b and ask whether those four stars have higher $\log(R'_{HK})$ values than the remaining 11 stars. We then repeat this test for a million different trials and find that we obtain the four largest $\log(R'_{HK})$ values for our non-inverted planets by chance only 0.13% of the time, corresponding to a 3.4σ result where the significance is limited by the small size of our sample.

We find that active G and K stars likely exhibit an enhancement of 4–7 in their Lyman α emission relative to quiet stars with similar effective temperatures and suggest that the increased UV flux from active stars destroys the high-altitude absorber responsible for the formation of temperature inversions. This theory is consistent with the sulfur model proposed by Zahnle et al. (2009) but could also be applied to a range of other scenarios. Because Ca II H & K and UV emission are only indirectly linked, definitive confirmation of this theory will require an estimate of the UV fluxes incident at the surfaces of these planets, taking into account both the spectral types and activity levels of their host stars as well as their orbital distances. Orbital eccentricity may also prove to be important, as planets such as XO-3 likely exist in a pseudo-synchronous spin state in which incident radiation is distributed more evenly over the surface than in the tidally locked case. If this is true, eccentric planets may require higher UV fluxes in order to suppress their dayside temperature inversions as compared to their tidally locked counterparts. We will address this issue in more detail in a follow-up paper, in which we examine the relationship between spectral type, Ca II H & K emission, and Lyman α emission and derive individual UV flux estimates for the transiting planets listed in Table 1.

Although *Spitzer* exhausted the last of its cryogen in 2009 May, the 3.6 and 4.5 μm channels on IRAC are still functioning at full sensitivity and the telescope continues to operate as part of an extended warm mission using those two channels. As part of this warm mission, we are currently executing a program to observe secondary eclipses of 19 additional transiting planets not observed during the cryogenic mission (ES program 60021, PI Knutson). When combined with the remaining unpublished secondary eclipse data from Spitzer's cryogenic mission and other ongoing warm mission programs (e.g., ES 60028, PI Charbonneau; DDT 60003, PI Harrington), data for 20–30 additional transiting planet systems should become available by summer 2011. We propose that the empirical scheme described in Section 4 can be used to provide an initial classification for these new systems, while the increasing availability of ground-based secondary eclipse detections as described above should help to provide better constraints for atmosphere models in cases where we are limited to the two shorter-wavelength *Spitzer* bands. Because active stars are less common in the sample of transiting planets (perhaps due to selection biases among the ground-based photometric surveys and the increased difficulty of radial velocity follow-up work for such systems), we suggest that the analysis of secondary eclipse data for planets orbiting active stars be given a high priority within the current large ongoing *Spitzer* programs.

We thank Geoff Marcy and Debra Fischer for their generous assistance in obtaining the Keck/HIRES spectra and deriving the SME values used in this analysis, as well as Lucianne Walkowicz, Kevin Zahnle, Mark Marley, Jonathan Fortney, Drake Deming, Jean-Michel Desert, and Adam Burrows for providing invaluable commentary on various aspects of this project. H.A.K. is supported by a fellowship from the Miller Institute for Basic Research in Science. We thank the observers who contributed to the data reported here. We gratefully acknowledge the efforts and dedication of the Keck Observatory staff, especially Scott Dahm, Hien Tran, and Grant Hill for support of HIRES and Greg Wirth for support of remote observing. A. W. H. gratefully acknowledges support from a Townes Post-doctoral Fellowship at the U. C. Berkeley Space Sciences Laboratory. Finally, the authors wish to extend special thanks to those of Hawai'ian ancestry on whose sacred mountain of Mauna Kea we are privileged to be guests. Without their generous hospitality, the Keck observations presented herein would not have been possible.

REFERENCES

Alonso, R., et al. 2009, A&A, 506, 353
Anderson, D. R., et al. 2010, A&A, 513, L3
Bailunas, S. L., et al. 1995, ApJ, 438, 269
Barman, T. S. 2008, ApJ, 676, L61
Beaulieu, J.-P., et al. 2010, ApJ, submitted, arXiv:1007.0324
Beerer, I. M., et al. 2010, ApJ, submitted
Borucki, W. J., et al. 2009, Science, 325, 709
Burrows, A., Budaj, J., & Hubeny, I. 2008, ApJ, 678, 1436
Burrows, A., Hubeny, I., Budaj, J., Knutson, H. A., & Charbonneau, D 2007, ApJ, 668, L171
Charbonneau, D., et al. 2005, ApJ, 626, 523
Charbonneau, D., et al. 2008, ApJ, 686, 1436
Christiansen, J. L., et al. 2010, ApJ, 710, 97
Deming, D. 2008, in Proc. IAU Symposium 253, Transiting Planets, ed. F. Pont, D. Sasselov, & M. Holman (Cambridge: Cambridge Univ. Press), 197
Deming, D., Harrington, J., Seager, S., & Richardson, L. J. 2006, ApJ, 644, 560

Deming, D., Seager, S., & Richardson, L. J. 2005, Nature, 434, 740
Deming, D., et al. 2010, ApJ, submitted
Duncan, D. K., et al. 1991, ApJS, 76, 383
Ehrenreich, D., et al. 2008, A&A, 483, 933
Fischer, D. A., & Valenti, J. 2005, ApJ, 622, 1102
Fontenla, J., Reichmann, E. J., & Tandberg-Hanssen, E. 1988, ApJ, 329, 464
Fortney, J. J., Lodders, K., Marley, M. S., & Freedman, R. S. 2008, ApJ, 678, 1419
Fortney, J. J., et al. 2006, ApJ, 652, 746
France, K., et al. 2010, ApJ, 712, 1277
Fressin, F., et al. 2010, ApJ, 711, 374
Gibson, N. P., et al. 2010, MNRAS, 404, L114
Gillon, M., et al. 2010, A&A, 511, A3
Gray, D. F. 2005, Observations and Analysis of Stellar Photospheres (3rd ed.; Cambridge: Cambridge Univ. Press)
Grillmair, C. J., et al. 2007, ApJ, 658, L115
Grillmair, C. J., et al. 2008, Nature, 456, 767
Harrington, J., et al. 2007, Nature, 447, 691
Hauschildt, P. H., Allard, F., & Baron, E. 1999, ApJ, 512, 377
Henry, T. J., Soderblom, D. R., Donahue, R. A., & Bailunas, S. L. 1996, AJ, 111, 439
Howard, A. W., et al. 2009, ApJ, 696, 75
Hubeny, I., Burrows, A., & Sudarsky, D. 2003, ApJ, 594, 1011
Isaacson, H., et al. 2010, ApJ, in press
Kashyap, V. L., Drake, L. J., & Saar, S. H. 2008, ApJ, 687, 1339
Knutson, H. A., et al. 2008, ApJ, 673, 526
Knutson, H. A., et al. 2009, ApJ, 691, 866
Landsman, W., & Simon, T. 1993, ApJ, 408, 305
Lecavelier des Etangs, A., et al. 2010, A&A, 514, A72
Leighton, R. B. 1959, ApJ, 130, 366
Liang, M.-C., Parkinson, C. D., Lee, A. Y., T., Yung, Y. L., & Seager, S. 2003, ApJ, 596, L247
Liang, M.-C., Seager, S., Parkinson, C. D., Lee, A. Y. T., & Yung, Y. L. 2004, ApJ, 605, L61
Line, M. R., Liang, M. C., & Yung, Y. L. 2010, ApJ, 717, 496
Linsky, J. L., et al. 2010, ApJ, 717, 1291
Livingston, W., Wallace, L., White, O. R., & Giampapa, M. S. 2007, ApJ, 657, 1137
López-Morales, M., et al. 2010, ApJ, 716, L36
Machalek, P., et al. 2008, ApJ, 684, 1427
Machalek, P., et al. 2009, ApJ, 701, 514
Madhusudhan, N., & Seager, S. 2009, ApJ, 707, 24
Marcy, G. W., & Butler, R. P. 1992, PASP, 104, 270
Noyes, R. W., Hartmann, L. W., Baliunas, S. L., Duncan, D. K., & Vaughan, A. H. 1984, ApJ, 279, 763
Nymeyer, S., et al. 2010, ApJ, submitted, arXiv:1005.1017
O'Donovan, F. T., et al. 2010, ApJ, 710, 1551
Poppenhaeger, K., Robrade, J., & Schmitt, J. H. M. M. 2010, A&A, 515, A98
Richardson, L. J., et al. 2007, Nature, 445, 892
Schrijver, C. J., Cote, J., Zwaan, C., & Saar, S. H. 1989, ApJ, 337, 964
Schrijver, C. J., Dobson, A. K., & Radick, R. R. 1992, A&A, 258, 432
Showman, A. P., et al. 2009, ApJ, 699, 564
Snellen, I. A. G., de Mooij, E. J. W., & Albrecht, S. 2009, Nature, 459, 543
Spiegel, D. S., & Burrows, A. 2010, ApJ, submitted, arXiv:1006.1660
Spiegel, D. S., Silverio, K., & Burrows, A. 2009, ApJ, 699, 1487
Stevenson, K. B., et al. 2010, Nature, 464, 1161
Swain, M. R., et al. 2009a, ApJ, 690, L114
Swain, M. R., et al. 2009b, ApJ, 704, 1616
Todorov, K., et al. 2010, ApJ, 708, 498
Valenti, J. A., Butler, R. P., & Marcy, G. W. 1995, PASP, 107, 966
Vidal-Madjar, A., et al. 2003, Nature, 442, 143
Vidal-Madjar, A., et al. 2004, ApJ, 604, L69
Vogt, S. S., et al. 1994, Proc. SPIE, 2198, 362
Wheatley, P. J., et al. 2010, ApJ, submitted, arXiv:1004.0836
Wilson, O. C. 1968, ApJ, 153, 221
Wood, B. E., et al. 2005, ApJ, 159, 118
Woods, T. N., et al. 2000, J. Geophys. Res., 105, 27195
Wright, J. T., Marcy, G. W., Butler, R. P., & Vogt, S. S. 2004, ApJS, 152, 261
Zahnle, K., Marley, M. S., & Fortney, J. J. 2010, ApJ, submitted, arXiv:0911.0728
Zahnle, K., Marley, M. S., Freedman, R. S., Lodders, K., & Fortney, J. J. 2009, ApJ, 701, L20